Magnetic Resonance in Medicine 70:1340–1346 (2013)

Transverse Relaxometry with Reduced Echo Train Lengths via Stimulated Echo Compensation

Md. Nasir Uddin, R. Marc Lebel,[†] and Alan H. Wilman*

Transverse relaxation (T_2) mapping has many applications, including imaging of iron accumulation in grey matter. Using the typical multiecho spin-echo sequence with long echo trains, stimulated echo compensation can enable T_2 fitting under conditions of variable radio frequency homogeneity arising from slice profile and in-plane radio frequency variation. Substantial reduction in the number of refocusing pulses could enable use at high magnetic fields where specific absorption rate is a major limitation, and enable multislice use with reduced incidental magnetization transfer at all field strengths. We examine the effect of reduced echo train lengths and multislice imaging on T_2 fitting using stimulated echo compensation applied to iron-rich subcortical grey matter in human brain at 4.7 T. Our findings indicate that reducing from 20 echoes to as few as four echoes can maintain consistent T_2 values when using stimulated echo compensation in grey and white matter, but not for cerebrospinal fluid. All territories produce marginal results when using standard exponential fitting. Savings from reduced echoes can be used to substantially increase slice coverage. In multislice mode, the resulting incidental magnetization transfer decreased brain signal but had minimal effect on measured T_2 values. **Magn Reson Med 70:1340–1346, 2013. © 2013 Wiley Periodicals, Inc.**

Key words: T_2; R_2 mapping; relaxometry; quantitative imaging; stimulated echo compensation; iron

Transverse relaxation (T_2) weighting provides a qualitative interpretation of disease and is used in almost all clinical MRI exams. Although T_2 weighting is typically sufficient for standard clinical depiction, T_2 quantification provides an absolute measure that could provide additional information on disease progression and state. In the brain, shortened T_2 times in subcortical grey matter (GM) may be indicative of iron accumulation or mineralization and appear to correlate with normal aging and with disease severity in multiple sclerosis and Parkinson's disease (1–9). In white matter (WM), T_2 fitting has proven to be valuable in demyelinating diseases to assess myelin content using the short myelin water T_2 component identified through multicomponent fitting (5,10–12); in GM the myelin component is much smaller (10). In addition to brain, quantification of single or multicomponent T_2 can characterize tissue throughout the human body (13–21), with applications such as iron accumulation in liver or collagen-bound water in cartilage (12,22–24).

Although other approaches exist, such as DESPO*T2* (25), the most common approach to T_2 measurement requires spin echo refocusing using a multiecho spin echo sequence, whereby T_2 values are calculated from the resulting, presumed exponential, decay curve (26). However, accurate exponential fitting of T_2 times with this approach requires perfect spin echo behavior, which is near-impossible to achieve when using slice selection due to imperfect slice profiles or when using high magnetic fields due to in-plane radio frequency (RF) interference (27). The presence of non-180° flip angles can lead to the generation of stimulated echoes, confounding the pure spin echo exponential decay (28). While numerous methods have been designed to minimize stimulated echo effects on the exponential decay, such as using twice-refocused adiabatic pulses (29), complex spoiler patterns (30) or extremely wide refocusing pulses (31), recent solutions have simply fit the complete spin response comprised of both spin echo and stimulated echo pathways. This idea of T_2 measurement by fitting the spin response, rather than introducing added complexities in the pulse sequence, was first proposed by Jones et al. (32), then elaborated on by Lebel and Wilman (33), with recent multicomponent application by Prasloski et al. (34). This method, known as stimulated echo compensation (SEC), can account for the nonideal nature of the refocusing pulses and enable use of more standard pulse sequences for T_2 quantification.

To date, SEC has been used with long echo trains of either 20 or 32 echoes (33,34). Performance of this method in the human brain with a small number of echoes and multislice imaging is unknown. Previous work with exponential fitting has demonstrated the limitations of reducing echo trains, where echo trains as low as 20 echoes were considered (35). Here, we explore vastly reduced echo numbers beginning at a maximum of 20 and reducing to as low as three, while maintaining consistent echo spacing. Particularly for high-field implementation, long echo trains are constrained by increased RF heating, with RF power deposition increasing with roughly the square of the magnetic field. Shorter echo trains would reduce RF heating substantially and enable multislice imaging with reduced losses from incidental magnetization transfer (MT). In human brain at 4.7 T, we examine the viability of extremely short echo trains and multislice imaging for single component T_2 fitting using SEC.

METHODS

MRI Acquisition

Two-dimensional multiecho spin-echo images of the human brain were obtained in single and multislice

Department of Biomedical Engineering, University of Alberta, Edmonton, Canada.

†*Present address:* General Electric Health Care, Calgary, Canada.

Grant sponsor: the Canadian Institutes of Health Research (CIHR) and the Natural Sciences and Engineering Research Council of Canada (NSERC).

*Correspondence to: Alan H. Wilman, Ph.D., Department of Biomedical Engineering, University of Alberta, 1098 Research Transition Facility, Edmonton, Alberta, Canada T6G 2V2. E-mail: wilman@ualberta.ca

Received 15 July 2012; revised 24 October 2012; accepted 29 October 2012.

DOI 10.1002/mrm.24568

Published online 16 January 2013 in Wiley Online Library (wileyonlinelibrary.com).

mode on a Varian Inova 4.7 T whole-body system. Axial, transverse relaxation maps of the human brain were obtained through the deep GM including the putamen, globus pallidus, and caudate nucleus. Fourteen healthy subjects (eight male, six female; mean age: 28 $\pm$ 2 years) were studied, all of whom gave written informed consent in accordance with institutional protocols. The typical scan parameters were 4000 ms TR, 10-ms echo spacing, 20 echo train length, 4-mm slice thickness, 8-mm slice gap, one or two slices, 50-kHz receiver bandwidth, and 256 $\times$ 145 imaging matrix, in-plane resolution 1.00 $\times$ 1.25 mm^2. Acquisition time was 5.2 min/image set. Different multislice coverage was tested ranging from two to eight slices, while maintaining the same total number of refocusing pulses by corresponding reduction of echo train length. Inter-echo spacing of 10 ms was maintained for all experiments. Excitation and refocusing angles were prescribed at 90° and 180°, respectively, with the refocusing pulse slice profile 1.75, 3.5, or 5 times wider than excitation. To minimize RF deposition, Gaussian pulses were used with durations for excitation and refocusing pulses of 4.00 ms (bandwidth of 672.5 Hz) and 2.29 ms (bandwidth of 1176.7 Hz), respectively. Images were collected with a four-element receive array (36) paired with a birdcage coil for transmit. Maximum gradient strength was 60 mT/m with a slew rate of 120 T/m/s.

T_2 Fitting and Analysis

Single-component T_2 fitting was carried out by fitting the full spin echo and stimulated echo response using SEC as previously described (33). This approach determines the T_2 and the relative flip angles for each voxel from examination of the spin response, beginning with knowledge of the RF pulse shapes and sequence timing. The spin response is calculated from the extended phase graph algorithm (28) and T_1 decay during the echo train is assumed negligible relative to T_2. The signal decay curves were fit on a pixel-by-pixel basis with SEC and with a standard exponential model for different numbers of consecutive echoes obtained both retrospectively and prospectively. Using the resulting T_2 maps, bilateral regions-of-interest were drawn on representative sections of iron-rich subcortical GM territories (including putamen, globus pallidus, and caudate nucleus), cortical GM, cerebrospinal fluid (CSF), partial volume, as well as WM. For multislice experiments, measurements were also performed to determine the influence of incidental MT on the resulting T_2 values.

RESULTS

Presence of stimulated echoes in the signal decay is easily recognized from an enhanced second echo as shown in Figure 1a. Because of high-field RF nonuniformity within the slice, the more central globus pallidus has less stimulated echo component than frontal WM because the refocusing flip angles are closer to the prescribed 180° near the image center. Figure 1b–f shows the population averaged T_2 from iron-rich deep GM (caudate, globus pallidus), WM territories (frontal, posterior internal capsule, and optic radiation), CSF, and partial volume (caudate with 20% CSF) for echo train reduction performed retrospectively using both SEC and exponential fits. The SEC is robust at most echo train lengths for GM and WM, where short echo trains are effective; however, for the long T_2 of CSF (Fig. 1h), overestimation is observed with echo trains below six. For WM regions of high myelin content, a slight underestimation of T_2 is observed with some short echo trains (Fig. 1f,g) due to a stronger weighting of the short myelin water T_2 over the longer components. The same effect is observed in the partial volume caudate with longer component CSF territory (Fig. 1e), where the average T_2 decreases slightly before increasing. For GM and frontal WM, consistent T_2 relaxation times are observed as the echo train is shortened, with only 2.4% maximum variation between 4 and 20 echoes. For posterior internal capsule (IC), this variation rises to 7.7% due to increased myelin content. Similar results were obtained with refocusing slice thickness 3.5 and 5 times larger than excitation thickness (data not shown).

For the standard exponential fit, a large variation in T_2 with echo train for all structures was observed especially with short echo trains. Signals due to stimulated echoes, which are particularly prominent in the second echo and present thereafter, lead to nonexponential decay producing increasing errors when echo trains are reduced when using an exponential fit. Even with long echo trains, exponential fit still overestimates the T_2 since stimulated echo pathways are not included; hence, T_2 convergence at higher numbers of echoes is not expected.

Using SEC, the fit produces both a T_2 and a normalized flip angle map. Figure 2 shows the normalized flip angle maps derived from the SEC algorithm for 2, 3, 4, and 20 echoes, respectively. The maps maintain consistency down to three echoes. Figure 3 presents typical R_2 maps ($1/T_2$) obtained using 20 echoes (left column) then reduced retrospectively to four echoes (middle column); the difference images (right column) suggest the SEC (a–c) remains accurate despite drastic reduction in echo train length, while the standard exponential fit (d–f) is highly dependent on the number of echoes in the fit.

Results from multislice imaging, where reduced echoes are translated into increased slice coverage, are shown in Table 1. The average T_2 values are presented using SEC for a single slice (20 echoes), two slices (20 echoes), four slices (10 echoes), and eight slices (5 echoes) from four subjects. Slice coverage and echo train length were varied under constant RF power deposition for the multislice acquisitions. Results from echo shortening in Table 1 follow the same trend as the retrospective case considered above, indicating minimal effect of incidental MT on the T_2 values. Example R_2 maps for various slices and echo numbers are shown in Figure 4, along with corresponding normalized flip angle maps obtained from the SEC fit.

Figure 5 examines incidental MT resulting from multislice T_2 imaging using the ratio of multislice to single-slice image SNR from an early echo image. Reductions in SNR between 5 and 17% were observed as the number of slices increases with corresponding echo train length reduction. The observed SNR reduction is negligible for CSF as expected. Note the expected dependence

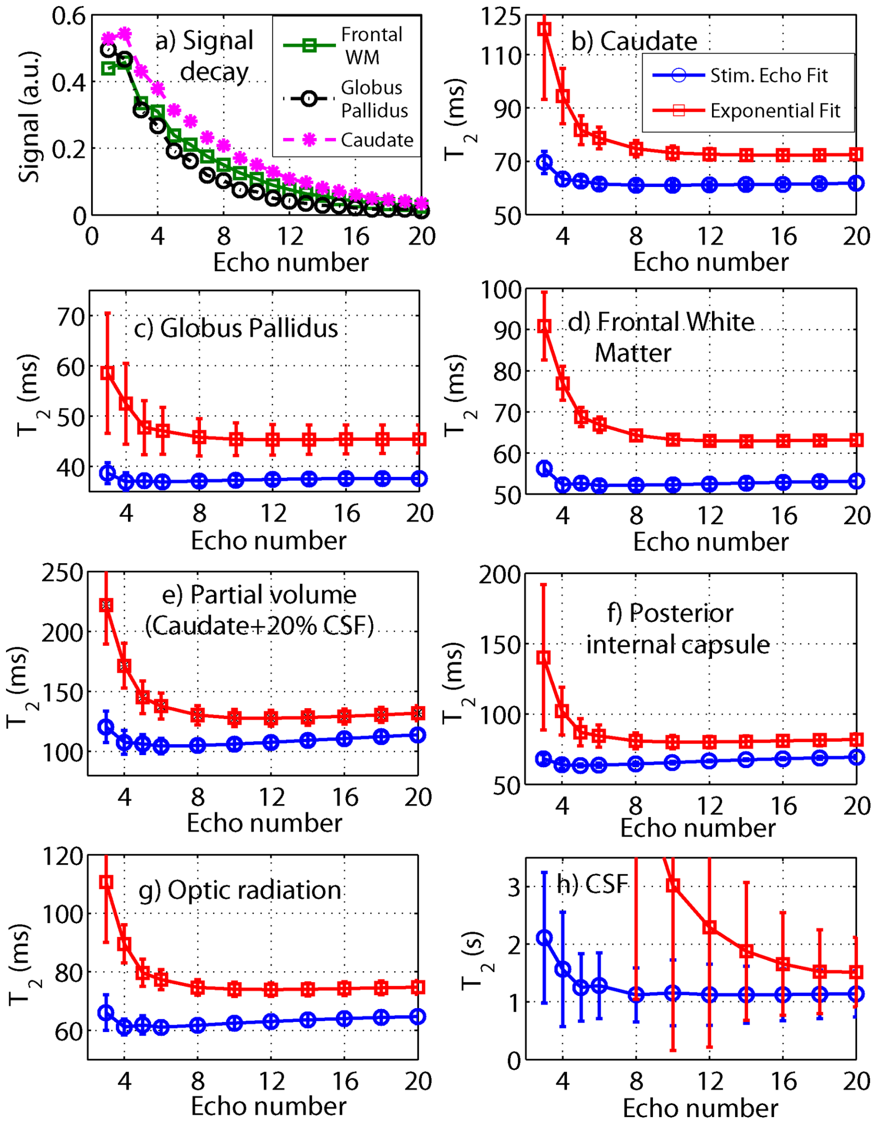

FIG. 1. **a**: Signal decay from one subject for three territories, (**b–h**) effect of number of echoes on the measured T_2 relaxation time using exponential fit or stimulated echo compensation averaged over 10 subjects in different brain regions. Error bars indicate intersubject standard deviations. Because of heterogeneous B_1 and slice-selective refocusing, the exponential fit provides erroneous results in all cases. In contrast, stimulated echo compensation provides good results for four or more echoes, except in the case of CSF, where additional echoes are needed.

on tissue type (WM versus GM) and on the flip angle (higher flip angle in center). The MT effects also have a T_1 dependence since the off-resonant slices are interleaved within the 4 s TR. For example, with two slices, off-resonant excitation occurs 2 s before acquisition.

DISCUSSION

With SEC, we have demonstrated that short echo trains as short as 4 can be used to constrain RF power and provide similar results to long echo trains for T_2 quantification of deep GM structures. Results in multicomponent

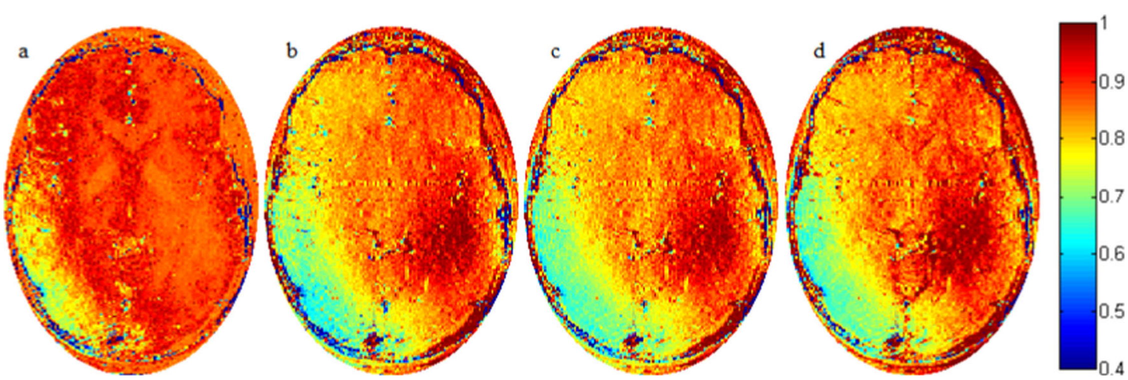

FIG. 2. Effect of number of echoes on normalized flip angle maps (retrospective): (**a**) two echoes, (**b**) three echoes, (**c**) four echoes, and (**d**) 20 echoes. Flip angle maps achieve stability with three or more echoes.

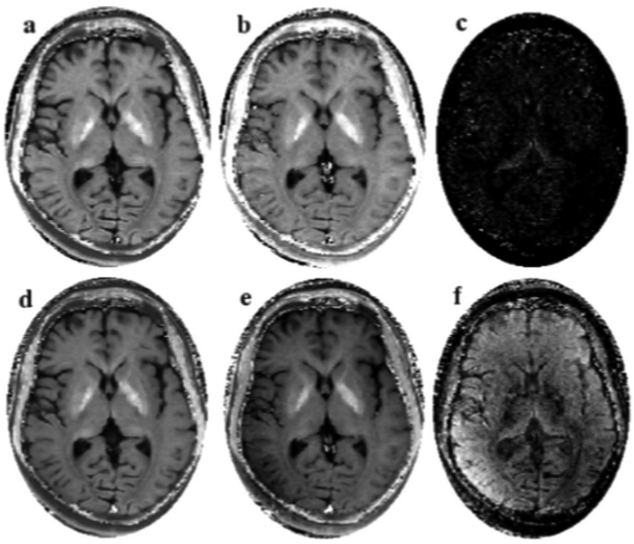

FIG. 3. In vivo R_2 maps: top row, stimulated echo fit; bottom row, exponential fit. In (**a**,**d**), 20 echoes are used, while (**b**,**e**) only four echoes. Difference maps are shown in (**c**,**f**) with stimulated echo (c) showing minimal change, but drastic differences for the exponential fit (f). Intensity scale is from 2.5 to 30 s^{-1} in images (a,b,d,e) and 0.68 to 7.5 s^{-1} for difference images (c,f).

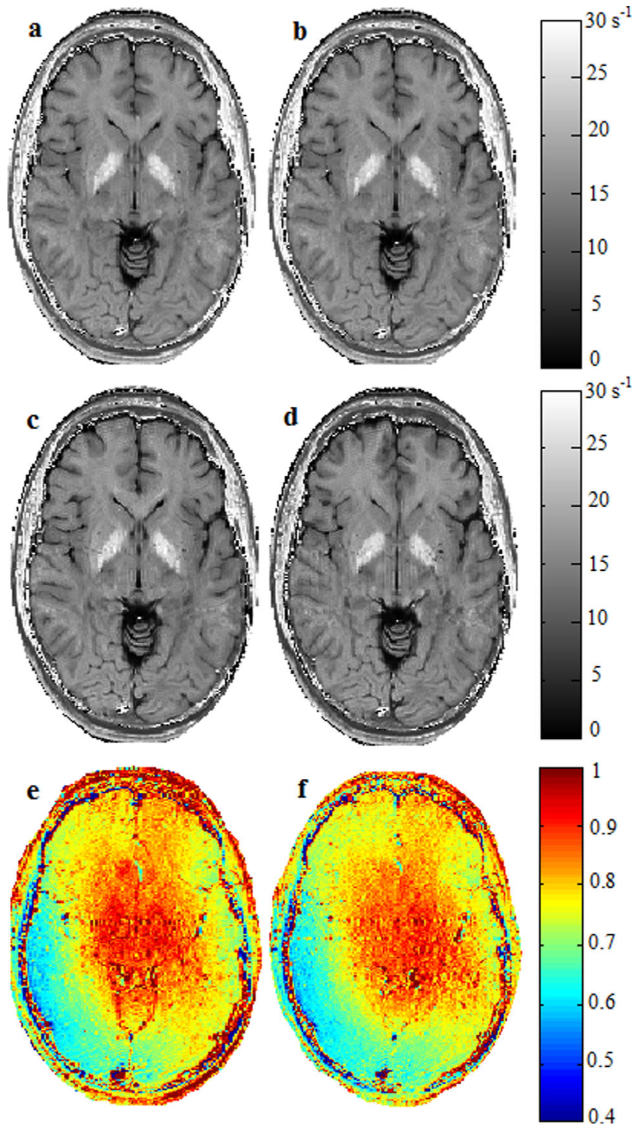

FIG. 4. In vivo R_2 maps using stimulated echo compensation: (**a**) one slice and 20 echoes, (**b**) two slices and 20 echoes, (**c**) four slices and 10 echoes, and (**d**) eight slices and five echoes. Corresponding normalized flip angle maps for (a) and (d) are shown in (**e**,**f**), respectively, demonstrating consistent flip angle estimation with short echo trains.

WM had slightly increased variability. Reduced echo train lengths can enable reduced RF power deposition or an increase in slice coverage and scan efficiency. However, given sufficient time and no RF heating constraints, long echo trains can produce better results, but are not always practical at high field, especially when more than one slice is required. Indeed, reduced echo trains can lead to less accuracy, especially in a low SNR environment (35). Optimal echo train length also depends on T_2 (37), with longer train length needed for longer T_2 values. Our results clearly indicate overestimation of the CSF T_2 when the number of echoes is reduced, but demonstrate excellent results for shorter T_2 values.

The multiecho spin-echo technique is sensitive to RF heterogeneity that can arise from through-plane RF variation from imperfect refocusing slice profiles or in-plane variation from RF interference effects. At 4.7 T used here, and at higher fields, in-plane heterogeneity is substantial for brain imaging (see Fig. 4e). Radio frequency heterogeneity can be improved somewhat by using RF shimming (38,39), or using multiple lobe, shaped, or double adiabatic refocusing pulses (40), which substantially increase RF power demands. Simply widening the thickness of the refocusing pulses relative to the excitation pulse can also improve the refocused slice profile (31), but limits potential for increased slice coverage. The SEC used here enables use of T_2 mapping at high magnetic field by accounting for RF field nonuniformity and enabling substantial echo reduction to minimize RF heating effects.

Increased slice coverage is necessary for future clinical application. We have demonstrated that savings in RF

Table 1
Average T_2 (ms) From Four Subjects for Different Number of Slices and Echoes Using the Stimulated Echo Fit

# of slices	# of echoes	Frontal WM	Caudate	Putamen	Globus pallidus	Posterior IC	Optic radiation	CSF
1	20	53.1 ± 1.5	61.0 ± 1.5	55.3 ± 1.5	37.0 ± 1.1	68.9 ± 2.5	65.4 ± 0.3	1132 ± 265
2	20	53.9 ± 0.6	60.6 ± 2.5	52.9 ± 3.1	37.0 ± 1.2	68.7 ± 2.9	65.3 ± 0.9	1202 ± 294
4	10	52.8 ± 0.9	61.2 ± 2.1	55.0 ± 1.6	36.6 ± 0.8	64.9 ± 2.3	63.1 ± 1.6	1518 ± 590
8	5	52.5 ± 1.1	62.9 ± 2.2	55.3 ± 2.2	35.0 ± 1.0	63.1 ± 2.7	60.3 ± 0.5	1619 ± 452

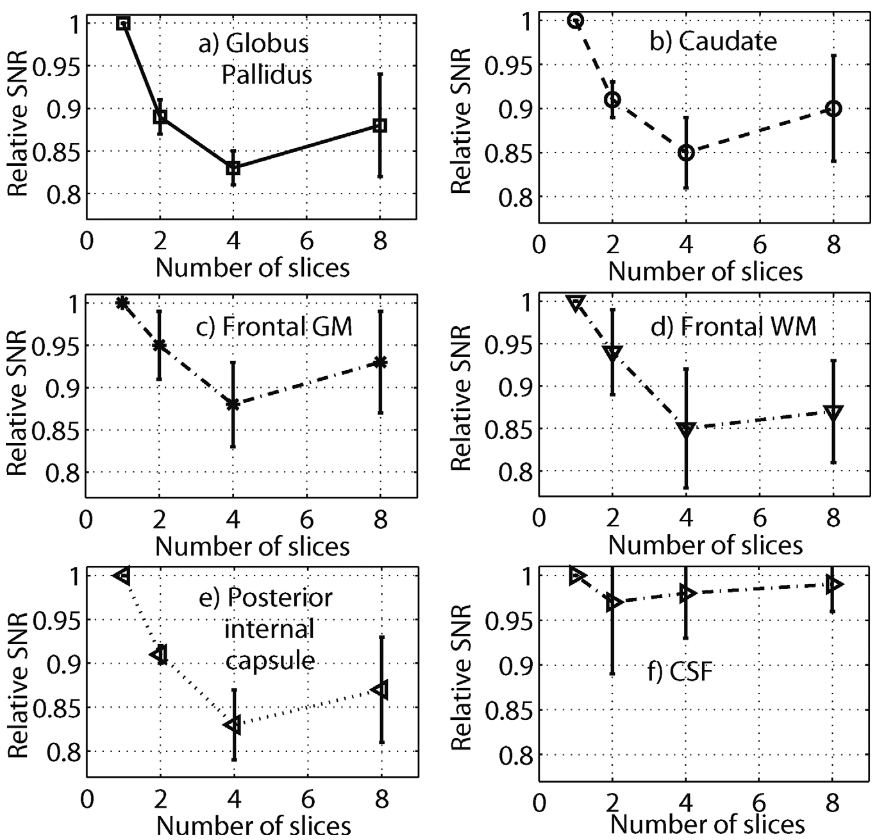

FIG. 5. Incidental MT effects illustrated through the relationship between relative SNR and the number of slices acquired in six brain territories averaged over four subjects. As slice number was increased past 2, the number of echoes was correspondingly decreased to maintain the same total number of refocusing pulses (slices-echoes: 1-20, 2-20, 4-10, 8-5). Error bars represent intersubject standard deviations.

power through echo shortening can be applied to increase the slice coverage, with similar T_2 results to single slice, even though there is signal reduction due to incidental MT effects (Fig. 5). We observed less than 15% SNR reductions from single slice to eight slices. Although SNR was lost in multislice mode due to incidental MT, it did not significantly affect the mean T_2 values for GM or WM and similar results were found for either retrospective echo shortening without MT effects (Fig. 1), or prospective echo shortening with increased slice number and incidental MT (Table 1). The effect of incidental MT on the T_2 fit was minimal partly due to the small number of off-resonant RF pulses used. Specifically in WM, the delay between off-resonant excitation and on-resonant acquisition minimized differential MT effects between myelin water and other pools due to exchange (41). The MT effects due to multislice interference were previously reported for human brain using fast spin echo sequences (42–45). Our incidental MT results are consistent with others (44,45). As expected, when the flip angle is similar, WM has greater MT than GM due to higher macromolecular content (42–48). Increased MT was observed from the posterior internal capsule because of higher myelin water content and greater flip angle in this more central region.

Increased slice coverage is also possible through single slab 3D imaging without incidental MT effects (49). This has been demonstrated at 3T using multiple spin echo 3D imaging with an eight-slice matrix (49); however, lengthy T_1 times at high field may limit imaging efficiency due to the need for long repetition times.

Our current implementation of SEC is based on the assumption that magnetization involved in alternate coherence pathways experiences negligible T_1 relaxation during the echo train, which provides accurate T_2 values for T_1/T_2 ratio above 10 (33), but for tissues with smaller T_1/T_2 ratios like CSF this assumption may provide underestimated T_2 values. Nevertheless, stimulated echo compensation still outperformed exponential fitting with CSF T_2 values using five echoes versus 20 echoes being 19% different with SEC and 2500% different for exponential fitting.

Throughout this work, we maintained a constant echo spacing of 10 ms similar to previous work (33,34) to control for diffusion effects between refocusing pulses (50,51) and to maintain signal from relatively short T_2 values that arise in regions of iron-laden ferritin in GM or very short T_2 from myelin water in WM. Simulations have shown that optimal interecho spacing and train length varies with T_2 values (37,52); however, there is a wide range of T_2 values across the human brain. Combining long interecho spacing with few echoes, has been shown to produce poor results in human brain (53); thus, a short-echo spacing is preferable.

In conclusion, it was shown that in contrast to standard exponential fitting, substantial shortening of the echo train can be achieved using SEC while maintaining accurate T_2 values at 4.7 T, where there is substantial RF inhomogeneity. Radio frequency power savings through echo reduction enabled accurate deep GM T_2 values using eight slices of five echoes each. Incidental MT was significant in multislice mode, but had minimal effect on the T_2 values. Thus, SEC with reduction of RF refocusing pulses can enable efficient use of T_2 mapping for high field or other applications where refocusing pulses are not ideal and RF power reductions are required.

REFERENCES

1. Khalil M, Langkammer C, Ropele S, et al. Determinants of brain iron in multiple sclerosis: a quantitative 3T MRI study. Neurology 2011; 77:1691–1697.
2. Lebel RM, Eissa A, Seres P, Blevins G, Wilman AH. Quantitative high-field imaging of sub-cortical gray matter in multiple sclerosis. Multiple Sclerosis J 2012;18:433–441.
3. Schenck JF, Zimmerman EA. High-field magnetic resonance imaging of brain iron: birth of a biomarker?NMR Biomed 2004;17:433–445.
4. Langkammer C, Krebs N, Goessler W, Scheurer E, Ebner F, Yen K, Fazekas F, Ropele S. Quantitative MR imaging of brain iron: a post-mortem validation study. Radiology 2010;257:455–462.
5. MacKay AL, Vavasour IM, Rauscher A, Kolind SH, Madler B, Moore GRW, Traboulsee AL, Li DKB, Laule C. MR relaxation in Multiple Sclerosis. Neuroimaging Clin N Am 2009;19:1–26.
6. Ge Y, Jensen JH, Lu H, Helpern JA, Miles L, Inglese M, Babb JS, Herbert J, Grossman RI. Quantitative assessment of iron accumulation in the deep gray matter of multiple sclerosis by magnetic field correlation imaging. Am J Neuroradiol 2007;28:1639–1644.
7. Bakshi R, Benedict RHB, Bermel RA, Caruthers SD, Puli SR, Tjoa CW, Fabiano AJ, Jacobs L. T_2 hypointensity in the deep gray matter of patients with multiple sclerosis—a quantitative magnetic resonance imaging study. Arch Neurol 2002;59:62–68.
8. Drayer B, Burger P, Hurwitz B, Dawson D, Cain J. Reduced signal intensity on MR images of thalamus and putamen in multiple sclerosis: increased iron content?Am J Roentgenol 1987;149:357–363.
9. Ceccarelli A, Rocca MA, Neema M, Martinelli V, Arora A, Tauhid S, Ghezzi A, Comi G, Bakshi R, Filippi M. Deep gray matter T_2 hypointensity is present in patients with clinically isolated syndromes suggestive of multiple sclerosis. Multiple sclerosis 2010;16:39–44.
10. Whittall KP, MacKay AL, Graeb DA, Nugent RA, Li DKB, Paty DW. In vivo measurement of T_2 distributions and water contents in normal human brain. Magn Reson Med 1997;37:34–43.
11. MacKay A, Laule C, Vavasour I, Bjarnason T, Kolind S, Madler B. Insights into brain microstructure from the T_2 distribution. Magn Reson Imaging 2006;24:515–525.
12. Laule C, Vavasour IM, Kolind SH, Traboulsee AL, Moore GRW, Li DKB, MacKay AL. Long T_2 water in multiple sclerosis: what else can we learn from multi-echo T_2 relaxation?J Neurol 2007;254: 1579–1587.
13. Dardzinski BJ, Mosher TJ, Li SZ, VanSlyke MA, Smith MB. Spatial variation of T_2 in human articular cartilage. Radiology 1997;205:546–550.
14. Perry J, Haughton V, Anderson PA, Wu Y, Fine J, Mistretta C. The value of T_2 relaxation times to characterize lumbar intervertebral disks: preliminary results. Am J Neuroradiol 2006;27:337–342.
15. Hosch W, Bock M, Libicher M, Ley S, Hegenbart U, Dengler TJ, Katus HA, Kauczor H-U, Kauffmann GW, Kristen AV. MR-Relaxometry of myocardial tissue - Significant elevation of T_1 and T_2 relaxation times in cardiac amyloidosis. Investigative Radiol 2007;42: 636–642.
16. White LM, Sussman MS, Hurtig M, Probyn L, Tomlinson G, Kandel R. Cartilage T_2 assessment: differentiation of normal hyaline cartilage and reparative tissue after arthroscopic cartilage repair in equine subjects. Radiology 2006;241:407–414.
17. Martin AJ, Poon CS, Thomas GM, Kapusta LR, Shaw PA, Henkelman RM. MR evaluation of cervical cancer in hysterectomy specimens: correlation of quantitative T_2 measurement and histology. J Magn Reson Imaging 1994;4:779–786.
18. Liney GP, Knowles AJ, Manton DJ, Turnbull LW, Blackband SJ, Horsman A. Comparison of conventional single echo and multi-echo sequences with a fast spin echo sequence for quantitative T_2 mapping: application to the prostate. J Magn Reson Imaging 1996;6: 603–607.
19. St Pierre TG, Clark PR, Chua-Anusorn W, Fleming AJ, Jeffrey GP, Olynyk JK, Pootrakul P, Robins E, Lindeman R. Noninvasive measurement and imaging of liver iron concentrations using proton magnetic resonance. Blood 2005;105:855–861.
20. Pai A, Li X, Majumdar S. A comparative study at 3 T of sequence dependence of T_2 quantitation in the knee. J Magn Reson Imaging 2008;26:1215–1220.
21. Maier CF, Tan SG, Hariharan H, Potter HG. T_2 quantitation of articular cartilage at 1.5 T. J Magn Reson Imaging 2003;17:358–364.
22. Papakonstantinou O, Kostaridou S, Maris T, Gouliamos A, Premetis E, Kouloulias V, Nakopoulou L, Kattamis C. Quantification of liver iron overload by T_2 quantitative magnetic resonance imaging in thalassemia: impact of chronic hepatitis C on measurements. J Pediatr Hematol Oncol 1999;21:142–148.
23. Horch RA, Nyman JS, Gochberg DF, Dortch RD, Does MD. Characterization of 1H NMR signal in human cortical bone for magnetic resonance imaging. J Magn Reson Med 2010;64:680–687.
24. Reiter DA, Lin P-C, Fishbein KW, Spencer RG. Multicomponent T_2 Relaxation Analysis in Cartilage. Magn Reson Med 2009;61:803–809.
25. Deoni SCL, Rutt BK, Peters TM. Rapid combined T_1 and T_2 mapping using gradient recalled acquisition in the steady state. Magn Reson Med 2003;49:515–526.
26. Poon CS, Henkelman RM. Practical T_2 quantitation for clinical applications. J Magn Reson Imaging 1992;2:541–553.
27. Vaughan JT, Garwood M, Collins C, Liu W, DelaBarre L, Adriany G, Andersen P, Merkle H, Goebel R, Smith M. 7T vs. 4T: RF power, homogeneity, and signal-to-noise comparison in head images. Magn Reson Med 2001;46:24–30.
28. Hennig J. Multiecho imaging sequences with low refocusing flip angles. J Magn Reson 1988;78:397–407.
29. Watanabe H, Takaya N, Mitsumori F. Non-uniformity correction of human brain imaging at high field by RF field mapping of B_1^+ and B_1^-. J Magn Reson 2011;212:426–430.
30. Does MD, Snyder RE. Multiecho imaging with suboptimal spoiler gradients. J Magn Reson 1998;131:25–31.
31. Pell GS, Briellmann RS, Waites AB, Abbott DF, Lewis DP, Jackson GD. Optimized clinical T_2 relaxometry with a standard CPMG sequence. J Magn Reson Imaging 2006;23:248–252.
32. Jones C, Xiang Q, Whittall K, MacKay A. Calculating T_2 and B_1 from decay curves collected with non-180 refocusing pulses. In Proceedings of the 11th Annual Meeting of ISMRM, Toronto, Canada, 2003. p. 1018.
33. Lebel RM, Wilman AH. Transverse relaxometry with stimulated echo compensation. Magn Reson Med 2010;64:1005–1014.
34. Prasloski T, Mädler B, Xiang QS, MacKay A, Jones C. Applications of stimulated echo correction to multicomponent T_2 analysis. Magn Reson Med 2012;67:1803–1814.
35. Anastasiou A, Hall LD. Optimisation of T_2 and M0 measurements of bi-exponential systems. J Magn Reson Imaging 2004;22: 67–80.
36. Carmichael DW, Thomas DL, De Vita E, Fernandez-Seara MA, Chhina N, Cooper M, Sunderland C, Randell C, Turner R, Ordidge RJ. Improving whole brain structural MRI at 4.7 Tesla using 4 irregularly shaped receiver coils. Neuroimage 2006;32:1176–1184.
37. Jones JA, Hodgkinson P, Barker AL, Hore PJ. Optimal sampling strategies for the measurement of spin-spin relaxation times. J Magn Reson Ser B 1996;113:25–34.
38. Tang L, Hue Y-K, Ibrahim TS. Studies of RF shimming techniques with minimization of RF power deposition and their associated temperature changes. Concepts Magn Reson Part B Magn Reson Eng 2011;39B:11–25.
39. Mao W, Smith MB, Collins CM. Exploring the limits of RF shimming for high-field MRI of the human head. Magn Reson Med 2006;56: 918–922.
40. Mitsumori F, Watanabe H, Takaya N. Estimation of brain iron concentration in-vivo using a linear relationship between regional iron and apparent transverse relaxation rate of the tissue water at 4.7T. Magn Reson Med 2009;62:1326–1330.
41. Vavasour IM, Whittall KP, Li DKB, MacKay AL. Different magnetization transfer effects exhibited by the short and long T_2 components in human brain. Magn Reson Med 2000;44:860–866.
42. Melki PS, Mulkern RV. Magnetization transfer effects in multislice RARE sequences. Magn Reson Med 1992;24:189–195.
43. Chang Y, Bae SJ, Lee YJ, Hwang MJ, Lee SH, Lee J, Lee SK, Woo S. Incidental magnetization transfer effects in multislice brain MRI at 3.0 T. J Magn Reson Imaging 2007;25:862–865.
44. Weigel M, Helms G, Hennig J. Investigation and modeling of magnetization transfer effects in two-dimensional multislice turbo spin echo sequences with low constant or variable flip angles at 3 T. Magn Reson Med 2010;63:230–234.

45. Lebel RM, Wilman AH. Time efficient fast spin echo imaging at 4.7 T with low refocusing angles. Magn Reson Med 2009;62:96–105.
46. Stanisz GJ, Odrobina EE, Pun J, Escaravage M, Graham SJ, Bronskill MJ, Henkelman RM. T_1, T_2 relaxation and magnetization transfer in tissue at 3T. Magn Reson Med 2005;54:507–512.
47. Santyr GE. Magnetization transfer effects in multislice MR imaging. J Magn Reson Imaging 1993;11:521–532.
48. Dixon WT, Engels H, Castillo M, Sardashti M. Incidental magnetization transfer contrast in standard multislice imaging. J Magn Reson Imaging 1990;8:417–422.
49. MacMillan EL, Madler B, Fichtner N, Dvorak MF, Li DKB, Curt A, MacKay AL. Myelin water and T_2 relaxation measurements in the healthy cervical spinal cord at 3.0T: repeatability and changes with age. Neuroimage 2011;54:1083–1090.
50. Bartha R, Michaeli S, Merkle H, Adriany G, Andersen P, Chen W, Ugurbil K, Garwood M. In vivo $^1(H_2O)$ T_2(dagger) measurement in the human occipital lobe at 4T and 7T by Carr-Purcell MRI: detection of microscopic susceptibility contrast. Magn Reson Med 2002;47: 742–750.
51. Ye FQ, Martin W, Allen PS. Estimation of brain iron in vivo by means of the interecho time dependence of image contrast. Magn Reson Med 1996;36:153–158.
52. Dula AN, Gochberg DF, Does MD. Optimal echo spacing for multi-echo imaging measurements of Bi-exponential T_2 relaxation. J Magn Reson 2009;196:149–156.
53. Whittall KP, MacKay AL, Li DKB. Are mono-exponential fits to a few echoes sufficient to determine T_2 relaxation for in vivo human brain?Magn Reson Med 1999;41:1255–1257.